Dostalek, J. F., L. D. Grasso, Y.-J. Noh, T.-C Wu, J. W. Zeitler, H. G. Weinman, A. E. Cohen., and D. T Lindsey, 2021: Using GOES ABI split-window radiances to retrieve daytime low-level water vapor for convective forecasting. *Electronic J. Severe Storms Meteor.*, **16** (2), 1–19.

Electronic Journal of
SEVERE STORMS METEOROLOGY

Using GOES ABI Split-Window Radiances to Retrieve Daytime Low-Level Water Vapor for Convective Forecasting

JOHN F. DOSTALEK, LEWIS D. GRASSO, YOO-JEONG NOH, AND TING-CHI WU
Cooperative Institute for Research in the Atmosphere,
Colorado State University, Fort Collins, Colorado

JON W. ZEITLER
NOAA/National Weather Service Forecast Office, Austin-San Antonio, Texas

HARRY G. WEINMAN
NOAA/National Weather Service Forecast Office, Miami, Florida

ARIEL E. COHEN
NOAA/National Weather Service Forecast Office, Pueblo, Colorado

DANIEL T. LINDSEY
NOAA/NESDIS/GOES-R, Fort Collins, Colorado

(Submitted 31 August 2020; in final form 11 April 2021)

ABSTRACT

A clear sky, daytime retrieval of low-level precipitable water vapor based on the single-layer approximation to the radiative transfer equation applied to three longwave window channels is described. The algorithm, which simultaneously retrieves skin temperature and air temperature as well, has the advantage of using satellite radiances only—no ancillary information is needed. Application of the method to Geostationary Operational Environmental Satellite (GOES)-16 Advanced Baseline Imager (ABI) radiance observations at 10.3, 11.2 and 12.3 μm demonstrates its utility in monitoring the location of low-level water vapor in the warm season, pre-convective atmosphere over the United States.

1. Introduction

In addition to instability and a source of lift, moisture is discussed by Doswell (1987) as a necessary ingredient in the development of convection. For days on which thunderstorms are expected to be severe, the moisture distribution is usually monitored in the context of a synoptic-scale convergence line, most notably a front or a dryline. In such cases it may be beneficial to monitor not only the surface moisture, but also the precipitable water in the near-surface layer. An increase in boundary-layer precipitable water in the vicinity of a convergence line could indicate the location of imminent convection even before clouds appear. Radiosondes provide a direct observation of the vertical distribution of moisture and are indispensable to National Weather Service (NWS) operations. However, features important to the development of convection can fit easily between the measurements, as weather balloons are launched from a network of stations that includes separations of several hundred kilometers. Furthermore, radiosonde observations typically are provided only twice daily, much coarser than the time scale on which severe convection operates. Alternatively, deepening low-level moisture can be inferred by surface moisture flux convergence (Waldstreicher 1989; Banacos and Schultz, 2005). To calculate surface moisture flux convergence, surface observations of moisture

Corresponding author address: John F. Dostalek, Cooperative Institute for Research in the Atmosphere, Colorado State University, 1375 Campus Delivery, Fort Collins, CO 80523-1375 E-mail: Jack.Dostalek@colostate.edu

are used in conjunction with the surface wind field. Although at a higher spatial and temporal resolution than the radiosonde network, surface observing stations of the contiguous United States can have a separation on the order of 10–100 km. Combined with a typical observation frequency of 1 h, the surface observing network is still coarser than the spatial and temporal scales of severe convection, which can be <20 km and <1 h, respectively (Orlanski 1975).

An additional source of moisture information beyond the in situ measurements of the surface observing network are remote measurements provided by sounding instruments aboard meteorological satellites (Menzel et al. 2018). Total precipitable water (TPW) over ocean surfaces has been measured by microwave instruments aboard polar-orbiting satellites (Grody 1976). Microwave radiation penetrates most clouds, but the orbits of these satellites provide any single location only two views per day. Combined with the roughly 50-km footprint, the data historically have been used for global observations rather than convective nowcasting.

Work is being done in this area, however. For example, Boukabara et al. (2011) introduced the Microwave Integrated Retrieval System (MiRS), a method to measure TPW over all surface types. To address the time gaps inherent in polar-orbiting satellite data, Kidder and Jones (2007) have blended data from many polar-orbiting satellites to create a TPW product that provides some time continuity. Wimmers and Velden (2011) use an alternate "advective blending" approach, combining TPW measurements with winds from the Global Forecast System model (Kalnay and Baker 1990) to eliminate the seams in the polar-orbiting data. Another microwave satellite moisture product displays upper-, middle-, and lower-level precipitable water (Leroy et al. 2016). The National Oceanic and Atmospheric Administration (NOAA) Unique Combined Atmospheric Processing System (NUCAPS, Nalli et al. 2018) combines both infrared and microwave data to produce retrievals of temperature and moisture that are available as individual profiles, or as gridded fields.

Despite these advances, the spatial and temporal resolution necessary for monitoring the pre-convective atmosphere is still achieved better with data from geostationary satellites. However, geostationary satellite retrieval techniques rely on measurements of infrared radiation. This limitation restricts the use of these techniques to generally cloud-free fields of view.

Techniques for measuring atmospheric moisture from geostationary platforms can be placed into one of three groups. The first group consists of algorithms employing a full retrieval of the vertical profile of water vapor, generally in terms of water vapor mixing ratio or dewpoint temperature (Ma et al. 1999). The vertical water vapor profile is retrieved simultaneously with the vertical temperature profile in a manner consistent with the radiative transfer equation (RTE). This retrieval is best performed using a sounding instrument such as the GOES Sounder (Schmit et al. 2002), which was included on the Geostationary Operational Environmental Satellite (GOES) 8–12 series (Menzel and Purdom 1994) and continued through GOES-15. Such instruments contain several channels in the carbon dioxide and water vapor absorption bands, providing temperature and moisture information throughout a substantial depth of the troposphere.

The Hyperspectral Environmental Suite was to be the next generation of geostationary sounder, providing much higher spectral resolution (Schmit et al. 2009), but was cancelled in 2007, leaving the newest series of GOES satellites (currently GOES-16 and -17) without a sounding instrument. Although not designed for the application, the Advanced Baseline Imager (ABI, Schmit et al. 2017; 2018) is capable of producing retrievals of temperature and moisture (Schmit et al. 2008, Lee et al. 2014, Schmit et al. 2019). Although the methods of this first group are consistent with radiative transfer theory, the ill-posed nature of the equations to be solved requires the use of ancillary data, which typically comes in the form of a first guess temperature and moisture profile from a numerical weather prediction model. In addition, to increase the signal to noise ratio, sounding instruments generally scan more slowly than imaging instruments. The GOES sounder viewed the continental United States (CONUS) once per hour.

The second group of algorithms relies on the varying degree to which water vapor attenuates radiation in the 10–12-μm range (Lindsey et al. 2012, 2014, 2018, Grasso et al. 2020). Although

considered a "window" region where extinction by the atmosphere is minimal, some absorption by water vapor does occur; the amount of absorption increases with increasing wavelength. Note that volcanic- and soil-derived aerosol detection algorithms use this same set of wavelengths (Ackerman 1997). Although volcanic matter is not typically expected over the continental United States, dust events do occur over the Plains states.

In a moist atmosphere with a positive lapse rate near the surface (typical of pre-convective daytime conditions) the brightness temperature at 12 μm is lower than that at 10 or 11 μm, with the difference related to the amount of low-level water vapor. This technique can also be used at night. In this case, lapse rates are typically negative, so the 12-μm brightness temperature will exceed that of the 10- or 11-μm channel. However, there is a period at both dawn and dusk where the lapse rate will be close to zero. At these times, the brightness temperature difference between the channels will be so small that the technique will not be able to measure moisture amounts. Because this approach requires only two channels, it does not require the use of a sounding instrument, and can take advantage of the faster scanning provided by an imager.

This computationally inexpensive method can be applied to imagery generated from the ABI's high speed scanning modes. However, even though this method is physically based, relying on the absorption characteristics of water vapor in the longwave infrared window, it does not consider other aspects of radiative transfer, most notably the contribution of the surface, which can often obscure the water vapor signal (Chesters et al. 1983, hereafter CUR). In addition, the value presented is a brightness temperature difference and not a typical measurement of moisture amount such as a dewpoint temperature, water vapor mixing ratio, or integrated water vapor amount.

The approaches of the techniques comprising the final group seek a middle ground between the first two. They attempt to preserve as much of the physical basis of a full retrieval as possible, yet still maintain the computational speed of the brightness temperature difference method. CUR, Kleespies and McMillin (1990), and Schroedter-Homscheidt et al. (2008) related the ratio of the transmittances at 12 and 11 μm to TPW. Jedlovec (1990) used a similar approach by using the square of the transmittance ratio. In the work of Guillory et al. (1993), the radiative transfer equation was manipulated and applied to 11 and 12 μm in a manner that resulted in a system of two equations that were simultaneously solved for the departure of the TPW and skin temperature from a mean value. Although these methods needed ancillary data in the form of regression coefficients (Kleespies and McMillin 1990; Jedlovec 1990; Schroedter-Homscheidt et al. 2008), a representative air temperature (CUR) or a first guess for TPW and skin temperature (Guillory et al. 1993), these techniques constitute a middle ground. They are not as computationally expensive as a full retrieval, yet are more sophisticated than the simple brightness-temperature difference. The problem arising from the skin temperature contribution is mitigated, and the moisture information is provided in physically meaningful units of a depth of water vapor.

At the time of these previous studies, imagers aboard geostationary satellites measured radiation from only two wavelengths in the split-window region—11 and 12 μm. The imaging instruments aboard some of the current geostationary satellites include a third split-window channel that measures radiation near 10 μm. Although employing many of the same assumptions used by CUR, the introduction of a third window channel makes possible the retrieval of low-level water vapor from satellite measurements without the need for ancillary information. This three-channel method is the subject of this paper and will be fully described in Section 2. Section 3 contains a validation of the technique, which includes a case study demonstrating its use. A discussion of the results is presented in Section 4, and a conclusion summarizes the work in Section 5.

2. Three channel determination of low-level water vapor

a. Theory

The proposed method starts with the single-layer approximation to the radiative transfer equation for wavelength λ assuming weak water-vapor absorption:

$$I_\lambda = \epsilon_\lambda B_\lambda(T_{skin})\tau_\lambda + B_\lambda\left(T_{air,\lambda}\right)(1-\tau_\lambda). \quad (1)$$

Except for T_{skin}, all of the variables in this equation depend on λ:

I_λ is the radiance emitted to space,

ϵ_λ is the surface emissivity, which will be assumed to be equal to unity as in CUR,

$B_\lambda(T)$ is the blackbody radiance at given temperature T,

T_{skin} is the surface skin temperature,

$T_{air,\lambda}$ is the temperature of the single layer of atmosphere, and

τ_λ is the transmittance from the surface to the top of the atmosphere.

Following CUR, the transmittance can be written in terms of a dry component and a wet component such that

$$\tau_\lambda = \tau_\lambda^{dry}\tau_\lambda^{wet}$$
$$\tau_\lambda^{dry} = exp[-\sec(\theta)k_\lambda]$$
$$\tau_\lambda^{wet} = exp[-\sec(\theta)(a'_\lambda W + a''_\lambda W^2 + a'''_\lambda W^3)] ,$$

where Θ is the satellite zenith angle, and W is the amount of water vapor in the single layer atmosphere. In the real atmosphere W represents the water vapor at low levels, as the weighting functions of wavelengths within a window region peak near the surface. As such, W will also be referred to as the boundary-layer precipitable water (BPW). The method of determining the values k_λ, a'_λ, a''_λ, and a'''_λ for the dry and wet optical depth calculation will be discussed in the next subsection.

Applying (1) to the 3 split-window wavelengths forms the basis of the technique for calculating the low-level water vapor. Unlike CUR, the radiative transfer equations will not be linearized to obtain equations in terms of brightness temperature, but will remain in the radiance formulation. In accordance with CUR however, it will be assumed that the single value T_{air} is valid for $T_{air,10}$, $T_{air,11}$, and $T_{air,12}$. The resulting set of equations for the variables W, T_{skin}, and T_{air} is:

$$B_{10}(T_{skin})\tau_{10}(W) + B_{10}(T_{air})[1 - \tau_{10}(W)] - I_{10} = 0 \quad (2a)$$
$$B_{11}(T_{skin})\tau_{11}(W) + B_{11}(T_{air})[1 - \tau_{11}(W)] - I_{11} = 0 \quad (2b)$$
$$B_{12}(T_{skin})\tau_{12}(W) + B_{12}(T_{air})[1 - \tau_{12}(W)] - I_{12} = 0 \quad (2c).$$

The respective subscripts 10, 11, and 12 have been used to denote the 10-, 11-, and 12-μm components of the set of three equations in three variables. The equations are nonlinear, removing the system from the realm of linear algebra with its predictable behaviors and ease of solutions. In this case Newton's (or Newton-Raphson's) method (Press et al. 1992) is used to solve the set of equations.

b. Application to GOES-ABI imagery

The set of equations 2a–2c comprises an algorithm that may be applied to any satellite instrument that measures radiation at the nominal wavelengths of 10, 11 and 12 μm. For monitoring time-evolving low-level water vapor for convective forecasting over the United States, geostationary imagery is the most appropriate. This work uses the ABI instrument on GOES-16, operating at 89.5°W during its checkout period (15 January–30 November 2017). The satellite was subsequently moved to the operational GOES-East location of (nominally) 75°W in December of 2017. The specific wavelengths of the ABI are 10.3, 11.2 and 12.3 μm.

The parameters k_λ, a'_λ, a''_λ, and a'''_λ for this work are calculated using output from a numerical weather prediction model and a radiative transfer model. Atmospheric profiles of temperature and moisture were generated at 59 levels from the surface to 25 km by the Regional Atmospheric Modeling System (RAMS, Cotton et al. 2003) for 8 May 2003 over a portion of the Great Plains. For this analysis cloud matter and precipitation were removed so the profiles of all 262 044 grid points could be processed. The profiles were then run in the Community Radiative Transfer Model (CRTM, Han et al. 2006). The dry absorbing gases in the CRTM are carbon dioxide and ozone. Carbon dioxide is a well-mixed gas and ozone is not an active absorber at the split-window wavelengths. The domain on that day contained a dryline, so the water-vapor amounts covered a wide range of values, with TPW spanning from a minimum of 4.5 mm to a maximum of 48.7 mm (Fig. 1).

For the dry optical depth, CUR remark that although a temperature dependence does exist, only the single, temperature independent value k_λ is necessary unless the temperature range of the entire globe is considered. CUR likely had in mind summertime conditions over the United States, as over the whole year the temperature variations over the continental United States can approach that of the earth as a whole. In any case, the monitoring of low-level moisture has perhaps its greatest application during the warm seasons, where the variation in temperatures across the United States is at its minimum.

Thus, only the temperature independent value k_λ is considered here. The value for k_λ at each of the three wavelengths of the algorithm, is given by the mean total optical depth of the RAMS grid points (Table 1).

Table 1: Dry and wet absorption coefficients derived from the CRTM using atmospheric profiles from RAMS model output.

λ (μm)	k_λ	a'_λ(mm^{-1})	a''_λ (mm^{-2})	a'''_λ(mm^{-3})
10.3	3.3702996×10^{-2}	$-7.6463096 \times 10^{-4}$	5.8735435×10^{-4}	$-5.6429571 \times 10^{-6}$
11.2	1.1643912×10^{-2}	$-8.3382942 \times 10^{-5}$	7.7797707×10^{-4}	$-7.4311011 \times 10^{-6}$
12.3	2.9299663×10^{-2}	5.7484123×10^{-3}	8.9924364×10^{-4}	$-8.2217621 \times 10^{-6}$

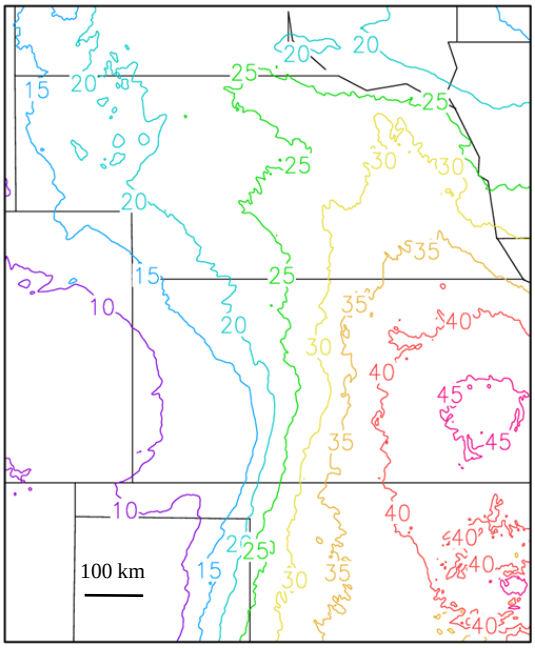

Figure 1: Total precipitable water (mm) from the RAMS model simulation used in the calculation of the coefficients used in the dry and moist transmittance. Contour interval is every 5 mm.

To get the coefficients a'_λ, a''_λ, and a'''_λ, the total optical depth due to water vapor as calculated by the CRTM is plotted against the TPW for each RAMS profile, and for each of the ABI wavelengths corresponding to the nominal 10-μm, 11-μm, and 12-μm requirements of the algorithm (Fig. 2). A best-fit curve passing through the origin defines the coefficients. CUR used a quadratic fit, but inspection of the scatterplots suggests a cubic fit better defines the relationship between total water vapor content and wet optical depth given here. The values of the three coefficients for the wet absorption for each of the three ABI wavelengths used (10.3, 11.2 and 12.3 μm) are given in Table 1.

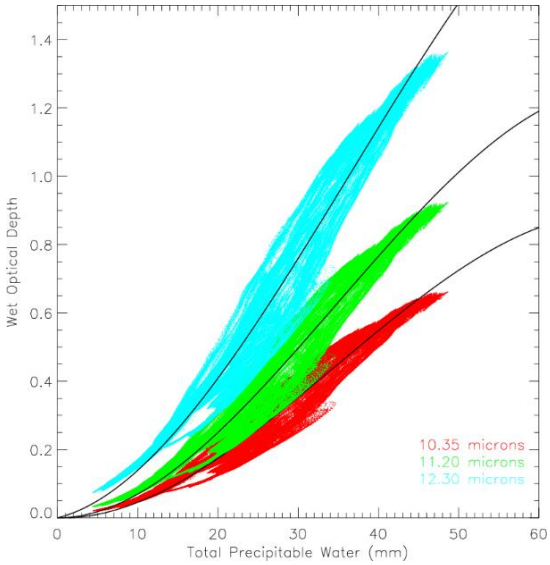

Figure 2: Scatterplot of wet optical depth versus total precipitable water for the 3 split-window channels of the GOES-16 ABI. The black lines represent the best-fit cubic polynomials passing through the origin for the scatterplots.

Although Li et al. (2009) demonstrate that satellite retrievals of moisture may be performed under thin cloud conditions, the evaluation of low-level water vapor W (i.e., BPW) by this algorithm is limited to clear-sky fields of view only. To increase the signal-to-noise ratio, the radiance assigned to a clear pixel is the mean of all clear pixels in the 3 × 3 box centered on the pixel. The cloudy pixels are identified using the NOAA Enterprise cloud mask (Heidinger et al. 2012), processed from the Clouds from AVHRR Extended (CLAVR-x) system (Heidinger 2013). For dates on which the NOAA Enterprise cloud mask is not available, a simple 10.3-μm brightness temperature threshold is used to determine cloudy pixels. Regardless of the sophistication of the cloud mask, some errors near the edges of thick clouds are evident in the imagery.

Newton's method requires that the variables be initialized with a first-guess value. The initial values assigned to the three variables are independent of pixel location: W = 15 mm, T_{skin} = 290K, T_{air} = 270K. The method produces what will be shown to be an accurate solution, and requires only a few seconds to run, more than adequate for the 5-min refresh rate of the GOES-East CONUS sector.

3. Validation

Validating the accuracy of the method is not straightforward. The weighting functions of the three wavelengths involved peak near the surface, so the label "boundary-layer precipitable water" is appropriate. The unit of mm is likewise appropriate, being a standard measure of integrated precipitable water. The difficulty lies in assigning a depth over which the measured water vapor exists. Being able to define a depth (e.g., hPa or m AGL) would greatly facilitate validation, because the vertical profile of water vapor measured from a radiosonde could be integrated from the surface to that depth and a direct comparison could be made to the quantity measured from satellite data. The weighting functions, however, do not have a constant depth associated with them. They change with the amount of water vapor, peaking higher with greater low-level moisture. Lacking a direct means of verification, two indirect approaches are presented to provide evidence that points to the validity of the algorithm. In the first approach, the relationship between BPW values and documented measures of water vapor are examined for consistency. Radiosonde data still provide the best measure of the vertical distribution of water vapor, but a comparison will also be made to a GOES TPW product. Second, a case study is presented to support the accuracy of the BPW product.

For the first comparison, the retrieved values of BPW were matched to the integrated precipitable water (IPW) observations from radiosonde data, computed from the surface to 3000 m at 50 m intervals. From the summer and fall of 2019, 338 midday (1700–2200 UTC) radiosonde launches from the CONUS were collected for comparison. Of these, 228 come from the special launches at NWS sites requested by NOAA's Storm Prediction Center (SPC) on days when severe weather is likely. The other 110 launches come from the U.S. Department of Energy's Atmospheric Radiation Measurement (ARM)-Southern Great Plains (SGP) site near Lamont, Oklahoma. For each IPW level, the root mean squared error (RMSE) was calculated (Fig. 3). A minimum of 3.8 mm exists at 1450 m, a height that reflects the near-surface peak of the window channel weighting functions. Therefore, the BPW represents the water vapor in approximately the lowest 1.5 km. As the figure shows however, the associated depth of integrated water vapor as measured by radiosondes is not constant. In fact, 17 of the 338 collocations (5%) had an altitude of integrated precipitable water >3000 m.

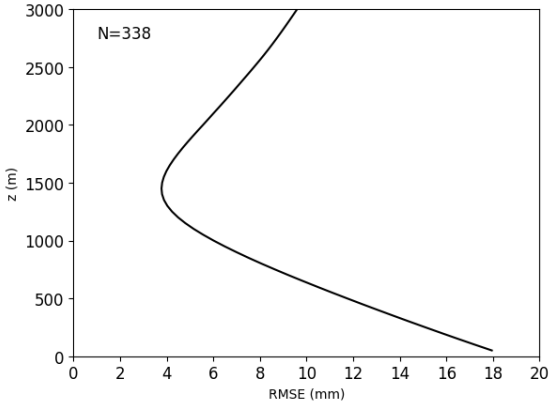

Figure 3: Root mean squared error between the retrieved BPW and the integrated water vapor observations (as a function of m AGL) from 338 collocated radiosonde launches over the CONUS during the summer and fall of 2019.

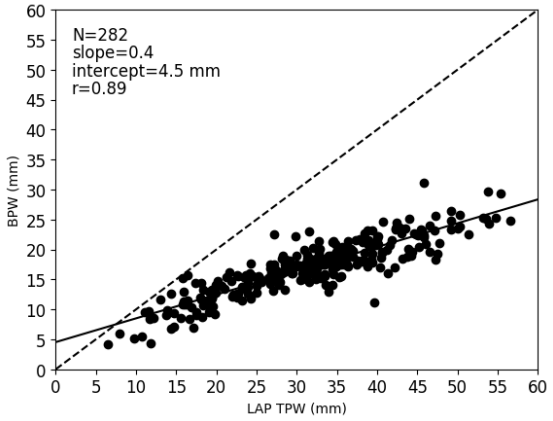

Figure 4: Scatterplot of the 282 matchups between the BPW values and the collocated values of the LAP TPW launches over the CONUS during the summer and fall of 2019. The dashed line is the one-to-one line, and the solid line is the best-fit line, the details of which are given in the upper-left corner of the plot.

Two hundred eighty-two of the 338 BPW/radiosonde matchups had an associated measure of TPW from the GOES-ABI suite of legacy atmospheric profile (LAP) products (Schmit et al. 2019). A scatterplot created from the two data sets is shown in Fig. 4. A strong correlation (r = 0.89) between the two products exists, with the BPW explaining 79% of the variance of the TPW. The TPW values exceed the BPW values, particularly at high TPW amounts. This relationship is consistent with the typical distribution of water vapor in the atmosphere. Most of the water vapor in an atmospheric column is usually near the surface. For dry atmospheres, very little water vapor is present at high altitudes, so the BPW will be essentially like the TPW. For moist atmospheres, the water vapor is generally not confined to the low levels only, meaning a greater fraction of the water vapor exists aloft, outside the sensitivity of the window channels on which the BPW product is based.

The second approach to providing evidence of the accuracy of the algorithm consists of analyzing imagery from a case example. On the morning of 15 June 2017, the United States was under the influence of three high-pressure systems and their associated air masses, as analyzed by the NOAA Weather Prediction Center (Fig. 5). Working from west to east, the high-pressure regions were centered over the Rocky Mountains (H_{RM}), over the southeastern United States (H_{SE}), and over New England (H_{NE}). Separating these high-pressure areas were two frontal systems anchored to a low-pressure area over Manitoba. The western front extended from Lake Superior southwest into New Mexico. Along the front two lesser lows were identified, one in eastern Nebraska and the other in southwestern Kansas. At the Texas-New Mexico border, the cold front intersected a dryline that extended south to the Texas-Mexico border. The eastern frontal system crossed the Great Lakes region to a low in western New York. From there it continued south through Pennsylvania and the mid-Atlantic states, turning east into the Atlantic Ocean from North Carolina.

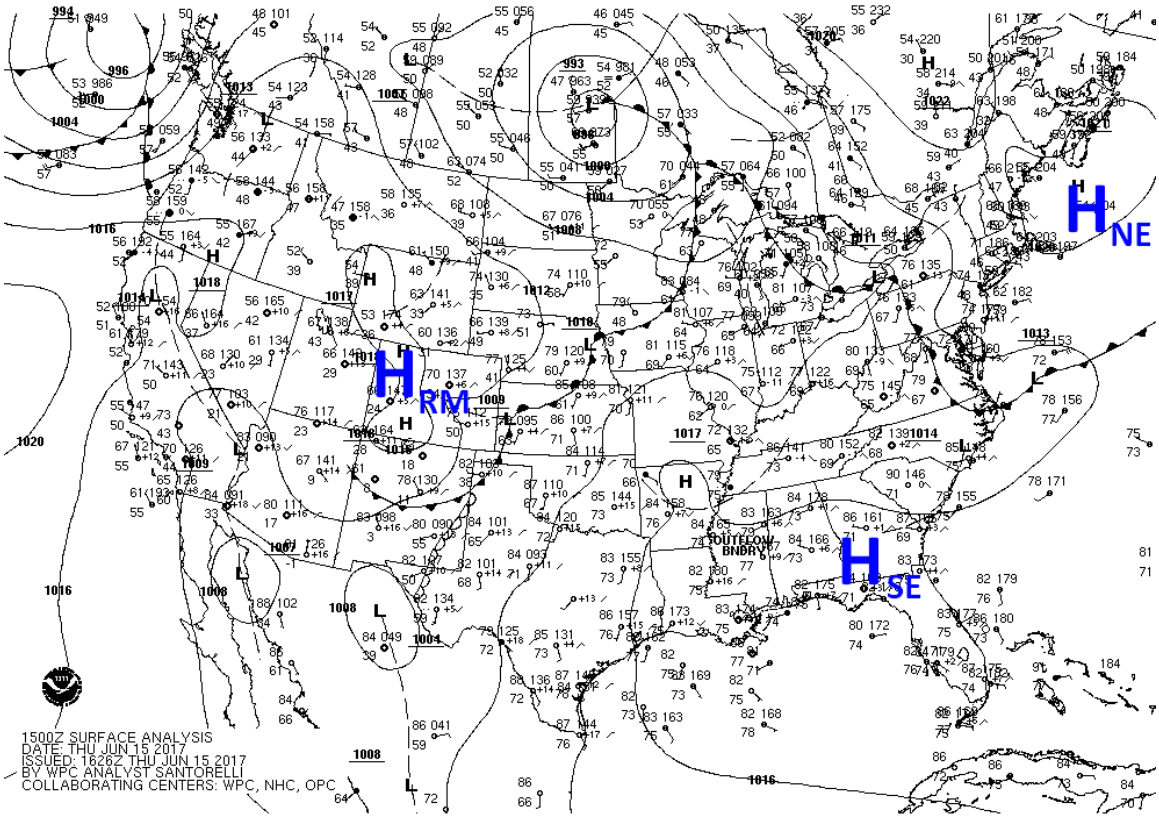

Figure 5: Conventional surface analysis from NOAA's Weather Prediction Center valid 1500 UTC, 15 June 2017. Labels for the three high pressure areas of interest (H_{RM}, H_{SE}, and H_{NE}) have been added to the analysis. *Click image to enlarge.*

The high-pressure regions can be broadly characterized using the accompanying surface observations. For this study, the surface dewpoint values are of most interest. The area covered by H_{RM} contained the driest air, with many stations recording dewpoint temperatures <4°C (40°F). H_{NE} was not as dry, but did have a few stations in Canada that reported dewpoints <4°C. Between these two relatively dry air masses lay the rather moist H_{SE}. Dewpoint temperatures > 18°C (65°F) were found over most of the area and reached as far north as Michigan.

Inasmuch as the low-level water vapor is a distinguishing characteristic among air masses, the BPW product from 1547 UTC 15 June 2017 (Fig. 6) does indicate the three regimes identified in the surface analysis. Over the Southwest, the BPW product indicates the lowest amounts of low-level water vapor over the United States, with values <2 mm in California, Utah, Arizona, and New Mexico, consistent with the dry air mass associated with H_{RM}. Across the cold front/dryline and into Texas a sharp moisture increase exists, with BPW >30 mm in the central part of the state. Some of the areas measuring BPW greater than 30 mm may be affected by unresolved cloud, but nevertheless the low-level water vapor displays a clear increase with respect to the Desert Southwest. Moisture continues to increase east and northeast from Texas. Clouds are more prevalent over the eastern United States, but the clear areas indicate a large area of high BPW over the Southeast and into the Ohio River Valley, extending as far north as Wisconsin and Michigan, conforming closely to the dewpoint field associated with H_{SE}. BPW values decrease over the northeastern United States, reflecting the moisture difference in the moist air mass of the southeast to the drier air mass associated with H_{NE}.

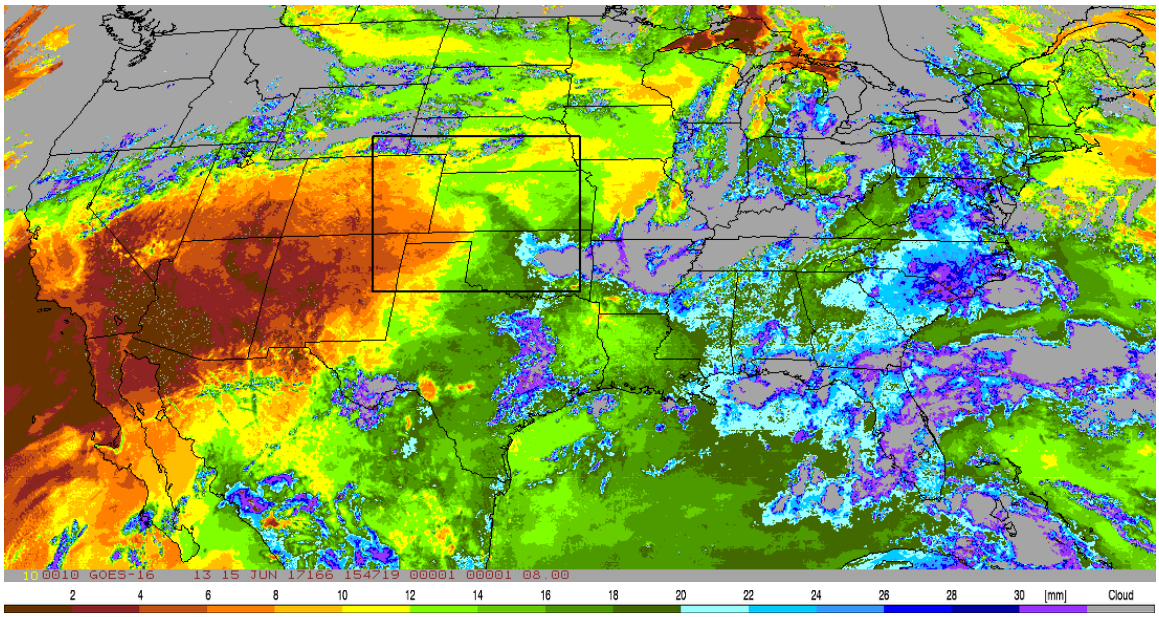

Figure 6: GOES-16 BPW product from 1547 UTC 15 June 2017. The color bar indicates the amount of low-level water vapor in mm. Clouds are masked out in gray, and the black box outlines the region shown in Fig. 7. *Click image to enlarge.*

In addition to broad-scale air mass identification, the BPW product has high-enough horizontal resolution to identify small-scale features. An example of such a feature can be seen in western Kansas, outlined in Fig. 6, and shown more closely in Fig. 7. NOAA's 1600 UTC Rapid Refresh (RAP) analysis contained an area of low pressure extending from southwest Kansas to the Texas Panhandle. To the east and north of the low, surface southerly and easterly winds advected water vapor around the leading edge of the system, with TPW values of up to 30 mm within the moisture axis. On the west side of the low, prevailing northwesterlies and southwesterlies accompanied the dry air, which was characterized by TPW values <20 mm. At that time, no clouds were present within the axis of high moisture (Fig. 7a). To the east of the low,

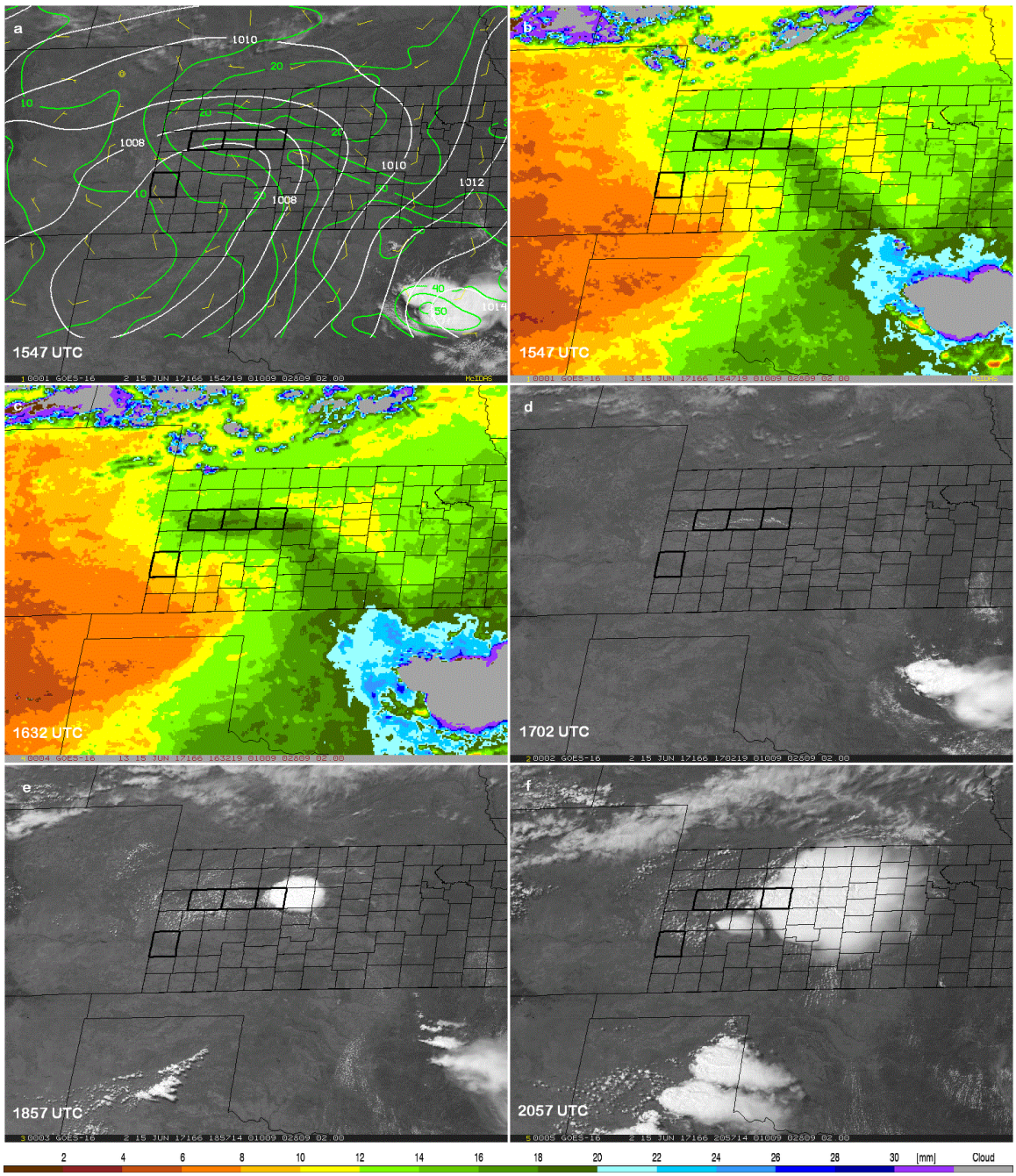

Figure 7: GOES-16 ABI images from 15 June 2017: a) 1547 UTC visible image with 1600 UTC RAP analysis fields of mean sea level pressure (hPa, white, contoured every 1 hPa), total precipitable water (mm, green, contoured every 5 mm), and 10-m wind barbs (full barb: 5 ms^{-1}, half barb: 2.5 ms^{-1}). b) 1547 UTC BPW image, c) 1632 UTC BPW image, d) 1702 UTC visible image, e) 1857 UTC visible image, and f) 2057 UTC visible image. Four Kansas counties are highlighted—Hamilton (southwest Kansas), and from west to east in west central Kansas: Logan, Gove, and Trego. The color bar below the image indicates the amount of BPW in mm. *Click image to enlarge.*

values of BPW just under 20 mm could be seen at 1547 UTC from south-central Kansas spreading to western Kansas. On the opposite side of the low, the air over southwestern Kansas contained <10 mm of BPW (Fig. 7b). Apart from depicting the juxtaposition of the moist and

dry air masses defining the dryline, both analyses indicated a pocket of slightly drier air to the north and east of the moisture maximum, although in slightly different locations. The RAP TPW analysis showed a local minimum <20 mm in north central to northwestern Kansas. The low-level water-vapor algorithm detected BPW values <12 mm in central Kansas.

Forty-five minutes later, an increase of water vapor near the moist axis was seen in the BPW product (Fig. 7c), with clouds becoming apparent in the visible imagery by 1702 UTC over western Kansas (Fig. 7d). By 1857 UTC a thunderstorm was evident over central Kansas (Fig. 7e). As the thunderstorm continued to grow (Fig. 7f), a second thunderstorm developed to its southwest. This storm did not last long, however, as it was likely hindered by the dry air in southwestern Kansas. The larger storm maintained a connection to the moist air and was therefore able to continue developing. Other convective development can be seen along the dryline in the Texas Panhandle and in the deeper moisture in eastern Oklahoma.

To highlight the spatial resolution of the BPW product, the counties of Kansas are displayed. Although sub-county variations in TPW are apparent in the RAP analysis, the BPW product shows these variations in much greater detail. For example, at 1547 UTC, BPW values greater than 12 mm were present in northeast Hamilton County, the single highlighted county along the Colorado border, dropping to 8 mm in the extreme southwestern portions (Fig. 7b). In addition, the axis of moisture around the north side of the low seen in the BPW is within Logan, Gove, and Trego counties. The RAP TPW analysis puts the axis one-half of a county to the south, along the southern borders of those counties (Fig. 7a). The line of clouds that did develop in association with this feature (Fig. 7d) formed within Logan, Gove, and Trego counties rather than on their southern border, more in line with the BPW maximum than the RAP TPW maximum.

4. Discussion

a. Forecaster perspective

Numerous efforts have been made to innovate meteorological services across the weather enterprise, and novel methods for assessing spatial distributions of atmospheric moisture (addressed herein) can extend directly to enhancing these services. For instance, comprehensive analyses identified by the NWS Operations Proving Ground (2019) suggest the proliferation of decision-support services that can be offered through a detailed assessment of the necessary conditions supporting convective development can have substantial effects on life and property. Strong situational awareness of the evolving three-dimensional mesoscale environment—that can be directly observed and analyzed via the methods articulated in the present study—can be foundational to enhancing the precision and accuracy of vital forecast information to core partners and customers of the NWS.

The vertical profile of moisture, and its variability in the horizontal plane, provides direct influence on the support or mitigation of convective initiation and its subsequent character. When mesoscale analysis of these fields is performed, leveraging the key concepts mentioned throughout this study, critical enhancements to forecast information can be offered to better promote life and property protection. Mesoanalysis is a key function of the human meteorologist, owing to the inherent and unique ability of the human to identify intricate patterns of the heterogeneities of meteorological parameters that influence convection.

Two examples—one local and one regional—highlight the importance of the low-level moisture distribution, and thus the utility of the high spatial and temporal resolution of the BPW product. First, the peninsular character of South Florida inherently establishes an elongated corridor of interface between marine and continental boundary layer. Mesoscale convergence along this corridor can influence both convective initiation and evolution. The exact character of this interface can be quite challenging to identify in real time, owing to the sparsely spaced observational systems. Thus, the previously addressed methods for moisture detection can offer novel support for assessing atmospheric moisture's forcing on convective behavior.

As another example, the evolution of boundary-layer moisture return (following intrusions of continental air masses) across the United States east of the Rockies also directly influences convective behavior. The return of this moisture, previously modified by fluxes atop of the Gulf of Mexico and Caribbean Sea, can be dramatic in both speed and magnitude—affecting

convective behavior from coastal states to Canada. The importance of moisture return, and mass-field heterogeneities, is relevant to convective forecasting year-round. In many circumstances, the conventional radiosonde network, and sometimes the surface-observing network, fail to resolve such fields fully. Sensors and techniques matching or exceeding the temporal and spatial scale of the features of interest (or their precursors), will provide the best depiction of the recent and current state of the atmosphere, and the prospects for accurate short-term prognosis of these features (Doswell 1986a,b).

Combined with existing observational tools and numerical weather prediction models, the BPW product, with spatial resolution on the order of kilometers and temporal resolution of 5 min, will yield a more integrated three-dimensional observational system for performing mesoscale environmental diagnosis and subsequent prognosis. This is especially valuable across data-sparse regions (e.g., Great Plains into northern Mexico), where surface observations are spatially limited, and real-time convective threat assessments are accompanied more frequently by higher-impact potential, while being both challenging and limited in predictability in many circumstances.

b. Possibility of using BPW in numerical modeling

In addition to aiding forecasters in identifying features related to convective activities, the BPW product may also provide value to numerical modeling of convective events via data assimilation. NOAA's operational RAP, which encompasses the High Resolution Rapid Refresh (HRRR) model is an hourly updated assimilation and model forecast system (Benjamin et al. 2016) that can facilitate this effort. The assimilation of satellite data into operational numerical weather prediction models is generally confined to using radiance information (Lin et al. 2017) and not temperature and moisture profiles or derived products. Data assimilation efforts in the research environment, however, may provide insight into the benefits of assimilating derived information versus the measured radiances. Furthermore, the BPW product can be also used as an independent verification dataset to evaluate results from data assimilation as well as model forecast output. Since BPW provides low-level water vapor information with a meaningful measurement in terms of mm, a direct comparison between BPW and simulated BPW computed from model output can be easily established.

c. Limitations and planned improvements

The BPW product depicts the low-level moisture in a manner that is consistent with the weighting functions of the split-window channels, as evident in the comparison with radiosonde data and the GOES LAP TPW product, as well as with the progression of thunderstorm development and maintenance. This was demonstrated in the convective development of 15 June 2017 over the south-central United States. The product's high spatial and temporal resolution track the locations of moisture needed for thunderstorm development.

Alternatively, the detailed location of the dry air may aid in determining where thunderstorms are *not* likely to develop or maintain their strength. The 15 June 2017 case provided an example of this possibility. A second cell that formed to the southwest of the main thunderstorm in western Kansas was not long lived. The dry airmass into which it moved likely contributed to its dissipation. However, the product has a limitation in that the BPW cannot be computed beneath clouds. Further work could be done comparing individual radiosondes with their associated BPW amounts to distinguish "typical" situations where the BPW is representative of low-level water vapor from the "atypical" situations for which the BPW covers a much larger depth of the atmosphere (i.e., the 5% of radiosondes mentioned in the discussion of Fig. 3). But the nationwide view of the clear-air distribution of low-level water vapor, on sub-county scales every 5 min, still provides valuable information.

Inspection of loops of the BPW product over the diurnal cycle reveal the need for additional algorithm development. Over water, the BPW displays a stable view of the low-level water vapor for all hours of the day. Over land, a noticeable drop in low-level water vapor occurs with the cooler temperatures of the evening and morning. Whether this drop is due to the assumptions used in the development of the system of equations, or in the implementation of Newton's method in its solution, will be addressed in future versions of the algorithm. Still, the BPW product was developed with

forecasting severe convection as the primary motivation, and severe thunderstorms are mostly a daytime phenomenon.

Additional improvements to the algorithm are also under consideration. Currently the algorithm assumes an emissivity of unity for all three wavelengths. Including a variable emissivity (e.g., Seemann et al. 2008) could result in a more accurate measure of low-level water vapor. Consideration must be given, however, to the current simplicity of the algorithm. The ABI also contains an additional window channel. Imagery at 8.4 μm potentially could be used in a 4-channel solution to the low-level water vapor problem, or as a substitute to the 10.3- or 11.2-μm channel. Absorption by SO_2 and surface emissivity differences with the 10–12-μm channels, however, may need consideration. Additional inputs might increase the complexity, primarily measured in computational speed, to a degree exceeding the benefit of the increased accuracy.

Application to imagers aboard other geostationary satellites would provide low-level water vapor measurements over other parts of the earth. In particular, the Advanced Himawari Imager aboard the Himawari satellites operated by the Japan Meteorological Agency (Bessho et al. 2016) and the Advanced Meteorological Imager aboard GEO-KOMPSAT-2A operated by the Korea Meteorological Administration (Chung et al. 2020) contain similar channels as the ABI. The Spinning Enhanced Visible and Infrared Imager (SEVIRI) aboard the Meteosat Second Generation satellites (Schmetz et al. 2002) of the European Organization for the Exploitation of Meteorological Satellites (EUMETSAT) provides the geostationary imaging over Europe and Africa. For this instrument, the previously mentioned 8-μm channel would be necessary, as the SEVIRI contains only two channels in the 10–12-μm range. A similar approach will be necessary for applying the product to the Flexible Combined Imager of the Meteosat Third Generation satellites (Holmlund et al. 2021).

5. Conclusion

In this study, an algorithm to estimate low-level precipitable water vapor was developed using information from three infrared window channels and applied to the GOES-16 ABI. The BPW algorithm is a promising solution to the decades-old problem of using information from the split-window channels on a geostationary imaging instrument to monitor low-level moisture, particularly in advance of thunderstorm outbreaks. Although a full vertical profile of water vapor has been available for many years from sounding instruments, the use of an imager provides a spatial and a temporal resolution more applicable to the forecasting of severe convection.

Previous attempts at measuring the low-level water vapor from a geostationary imager (apart from the retrieval of a full temperature and moisture profile) used only two channels, one near 11 μm and another near 12 μm, as those were the only split-window channels available. These two-channel techniques are easily produced and able to provide some information on the distribution of low-level water vapor but include notable drawbacks. For example, they do not account adequately for the variations in skin temperature. Additionally, the value computed is a brightness-temperature difference and not a commonly used metric of moisture amount, such as a dewpoint temperature, mixing ratio amount, or depth of water vapor. More advanced two-channel techniques are available to mitigate the skin-temperature obstacle, and to provide a more meaningful measure of moisture, mm of water vapor, but they require the introduction of ancillary data.

With the advent of the GOES-R series of satellites came the next-generation imager, the ABI, with an additional window channel at 10.3 μm. By using wavelengths at 10, 11, and 12 μm, a geostationary imager can retrieve the low-level water vapor in a manner that accounts for the spatial variations in skin temperature, without the use of ancillary data. This technique applies the single-layer radiative transfer equation to the three wavelengths, using Newton's method to compute the low-level water vapor, the skin temperature and the air temperature simultaneously. From comparison with radiosonde measurements over the continental United States, the algorithm produces a depth of water vapor generally equal to integrating the moisture profile from the surface to around 1.5 km, a height consistent with the shape of the split-window weighting functions. The BPW product also correlates well with the GOES-16 LAP TPW product, explaining 79% of its variance. Finally, a case study example over the United States provides evidence to the veracity of the method. The BPW product outlined the

general distribution of low-level moisture, matching the patterns produced by surface observations and output from a numerical weather prediction model. At smaller scales, an increase in the depth of moisture, like what would be expected in a region of moisture flux convergence, preceded the development of cumulus clouds over western Kansas that eventually formed into a thunderstorm.

Several improvements to the BPW algorithm are planned. Most important is the ability to retrieve BPW accurately over land during the cooler times of the day. Other potential improvements may come from incorporating surface emissivity variations and including information from the 8.4-μm channel. Finally, an improvement in the extent of low-level water vapor measurements can come from applying the technique to the data from imaging instruments aboard other geostationary satellites.

ACKNOWLEDGMENTS

The authors would like to thank Scott Fulton (Department of Mathematics, Clarkson University) for providing valuable input on the use of Newton's method, and Robert DeMaria (Cooperative Institute for Research in the Atmosphere) for advice on programming the algorithm. Gary Jedlovec (NASA-Marshall Space Flight Center) pointed out additional references on the use of the split-window channels in the determination of low-level water vapor. The thoughtful reviews of Rebekah Esmaili and Tim Schmit provided valuable insight for improving the manuscript. The views, opinions, and findings contained in this report are those of the authors and should not be construed as an official National Oceanic and Atmospheric Administration or U.S. government position, policy or decision. This project was supported under NOAA Grant NA19OAR4320073.

REFERENCES

Ackerman, S. A., 1997: Remote sensing aerosols using satellite infrared observations. *J. Geophys. Res.*, **102**, 17 069–17 079.

Banacos, P. C., and D. M. Schultz, 2005: The use of moisture flux convergence in forecasting convective initiation: Historical and operational perspectives. *Wea. Forecasting*, **20**, 351–366.

Benjamin, S. G., and Coauthors, 2016: A North American hourly assimilation and model forecast cycle: The Rapid Refresh. *Mon. Wea. Rev.*, **144**, 1669–1694.

Bessho, K., and Coauthors, 2016: An introduction to *Himawari-8/9*—Japan's new-generation geostationary meteorological satellites. *J. Meteor. Soc. Japan*, **94**, 151–183.

Boukabara, S. A., and Coauthors, 2011: MiRS: An all-weather 1DVAR satellite data assimilation and retrieval system. *IEEE Trans. Geosci. Remote Sens.*, **49**, 3249–3272.

Chesters, D., L. W. Uccellini, and W. D. Robinson, 1983: Low-level water vapor fields from the VISSR atmospheric sounder (VAS) "split window" channels. *J. Climate Appl. Meteor.*, **22**, 725–743.

Chung, S.-R., M.-H. Ahn, K.-S. Han, K.-T. Lee, and D.-B. Shin, 2020: Meteorological products of Geo-KOMPSAT 2A (GK2A) Satellite. *Asia-Pacific J. Atmos. Sci.*, **56**, 185, https://doi.org/10.1007/s13143-020-00199-x.

Cotton, W. R., and Coauthors, 2003: RAMS 2001: Current status and future directions. *Meteor. Atmos. Phys.*, **82**, 5–29.

Doswell, C. A. III, 1986a: The human element in weather forecasting. *Natl. Wea. Dig.*, **11**, 6–18.

——, 1986b: Short range forecasting. *Mesoscale Meteorology and Forecasting*, P. S. Ray, Ed., Amer. Meteor. Soc., 689–719.

——, 1987: The distinction between large-scale and mesoscale contribution to severe convection: A case study example. *Wea. Forecasting*, **2**, 3–16.

Grasso, L. and Coauthors, 2020: Application of the GOES-16 Advanced Baseline Imager: Morphology of a preconvective environment on 17 April 2019. *Electronic J. Severe Storms Meteor.*, **15** (2), 1–24.

Grody, N. C., 1976: Remote sensing of atmosphere water content from satellites using microwave radiometry. *IEEE Trans. Antennas Propagat.*, **AP-24**, 155–162.

Guillory, A. R., G. J. Jedlovec, and H. E. Fuelberg, 1993: A technique for deriving column-integrated water content using VAS split-window data. *J. Appl. Meteor.*, **32**, 1226–1240.

Han, Y., P. van Delst, Q. Liu, F. Weng, B. Yan, R. Treadon, and J. Derber, 2006: Community Radiative Transfer Model (CRTM): Version 1, NOAA Tech. Rep. NESDIS 122, 33 pp. [Available online at https://repository.library.noaa.gov/view/noaa/1157.]

Heidinger, A. K., 2013: ABI cloud height. Version 3.0, NOAA/NESDIS/STAR algorithm theoretical basis doc., 79 pp. [Available online at https://www.star.nesdis.noaa.gov/goesr/docs/ATBD/Cloud_Height.pdf.]

——, A. T. Evan, M. J. Foster, and A. Walther, 2012: A naïve Bayesian cloud-detection scheme derived from CALIPSO and applied within PATMOS-x. *J. Appl. Meteor. Clim.*, **51**, 1129–1144.

Holmlund, K., and Coauthors, 2021: Meteosat Third Generation (MTG): Continutation and innovation of observation from geostationary orbit. *Bull. Amer. Meteor. Soc.*, **102**, 1–71.

Jedlovec, G. J., 1990: Precipitable water estimation from high-resolution split window radiance measurements. *J. Appl. Meteor.*, **29**, 863–877.

Kalnay, M. K., and W. E. Baker, 1990: Global numerical weather prediction at the National Meteorological Center. *Bull. Amer. Meteor. Soc.*, **71**, 1410–1428.

Kidder, S. Q, and A. S. Jones, 2007: A blended satellite total precipitable water product for operational forecasting. *J. Atmos. Oceanic Technol.,* **24,** 74–81.

Kleespies, T. J. and L. M. McMillin, 1990: Retrieval of precipitable water from observations in the split window over varying surface temperatures. *J. Appl. Meteor.*, 29, 851–861.

Lee, Y.-K., Z. Li, J. Li, and T. J. Schmit, 2014: Evaluation of the GOES-R LAP retrieval algorithm using the *GOES-13* Sounder. *J. Atmos. Oceanic Technol.*, **31**, 3–19.

Leroy, A., K. K. Fuell, A. L. Molthan, G. J. Jedlovec, J. M. Forsythe, S. Q. Kidder, and A. S. Jones, 2016: The operational use and assessment of a layered precipitable water product for weather forecasting. *J. Oper. Meteor.*, **4**, 22–33.

Li, Z., J. Li, W. P. Menzel, J. P. Nelson III, T. J. Schmit, E. Weisz, and S. A. Ackerman, 2009: Forecasting and nowcasting improvement in cloudy regions with high temporal GOES Sounder infrared radiance measurements. *J. Geophys. Res.*, **114**, D09216, doi:10.1029/2008JD010596.

Lin, H., S. S. Weygandt, S. G. Benjamin, and M. Hu, 2017: Satellite radiance data assimilation within the hourly updated Rapid Refresh. *Wea. Forecasting*, **32**, 1723–1287

Lindsey, D. T., T. J. Schmit, W. M. MacKenzie Jr., C. P. Jewitt, M. M. Gunshor, and L. Grasso, 2012: 10.35 μm: Atmospheric window on the GOES-R Advanced Baseline Imager with less moisture attenuation. *J. Appl. Remote Sens.*, **6** (1), 063598, doi:10.1117/1.JRS.6.0635 98.

——, L. Grasso, J. F. Dostalek, and J. Kerkmann, 2014: Use of the GOES-R split window difference to diagnose deepening low-level water vapor. *J. Appl. Meteor. Clim*., **53**, 2005–2016.

——, D. T., D. Bikos, and L. Grasso, 2018: Using the GOES-16 split window difference to detect a boundary prior to cloud formation. *Bull. Amer. Meteor. Soc*., **99**, 1541–1544.

Ma, X. L., T. J. Schmit, and W. L. Smith, 1999: A nonlinear physical retrieval algorithm—Its application to the GOES-8/9 sounder. *J. Appl. Meteor.*, **38**, 501–513.

Menzel, W. P. and J. F. W. Purdom, 1994: Introducing GOES-I: The first of a new generation of geostationary operational environmental satellites. *Bull. Amer. Meteor. Soc.*, **75**, 757–782.

——, T. J. Schmit, P. Zhang, and J. Li, 2018: Satellite-based atmospheric infrared sounder development and applications. *Bull. Amer. Meteor. Soc*., **99**, 583–603.

Nalli, N. R., and Coauthors, 2018: Validation of atmospheric profile retrievals from the SNPP NOAA-Unique combined atmospheric processing system. Part 1: Temperature and moisture. *IEEE Trans. Geosci. Remote Sens.*, **56**, 180–190.

NWS Operations Proving Ground (OPG), 2019: Connecting expert mesoanalysis to enhanced collaborative severe weather IDSS: An OPG-SPC proof-of-concept experiment. 35 pp. [Available online at https://vlab.ncep.noaa.gov/documents/214451/5286029/MBC+Report.pdf/66875bc3-dc16-4985-c8dc-491f75e2af45?t=1572447395712.]

Orlanski, I., 1975: A rational subdivision of scales for atmospheric processes. *Bull. Amer. Meteo. Soc.*, **56**, 527–530.

Press, W. H., S. A. Teukolksy, W. T. Vetterling, and B. P. Flannery, 1992: *Numerical Recipes in Fortran 77: The Art of Scientific Computing.* Cambridge University Press, 933 pp.

Schmetz, J., P. Pili, S. Tjemkes, D. Just, J. Kerkmann, S. Rota, and A. Ratier, 2002: An introduction to Meteosat Second Generation (MSG). *Bull. Amer. Meteor. Soc.*, **83**, 977-992.

Schmit, T. J., W. F. Feltz, W. P. Menzel, J, Jung, A. P. Noel, J. N. Heil, J. P. Nelson III, and G. S. Wade, 2002: Validation and use of GOES sounder moisture information. *Wea. Forecasting*, **17**, 139–154.

——, J. Li, J. Gurka, M.D. Mitch, K.J. Schrab, J. Li, and W.F. Feltz, 2008: The GOES-R Advanced Baseline Imager and the continuation of current sounder products. *J. Appl. Meteor. Clim.*, **47**, 2696–2711.

——, ——, S. A. Ackerman, and J. J. Gurka, 2009: High-spectral- and high-temporal-resolution infrared measurements from geostationary orbit. *J. Atmos. Oceanic Technol.*, **26,** 2273–2292.

——, P. Griffith, M. W. Gunshor, J. M. Daniels, S. J. Goodman, and W. J. Lebair, 2017: A closer look at the ABI on the GOES-R series. *Bull. Amer. Meteor. Soc.*,**98,** 681–698.

——, S. S. Lindstrom, J. J. Gerth, and M. W. Gunshor, 2018: Application of the 16 spectral bands on the Advanced Baseline Imager (ABI*). J. Operational Meteor.*, **6** (4), 33–46.

——, T. J., J. Li, S. J. Lee, Z. Li, R. Dworak, Y.-K. Lee, M. Bowlan, J. Gerth, G. D. Martin, W. Straka, K. C. Baggett, and L. Cronce, 2019: Legacy atmospheric profiles and derived products from GOES-16: Validation and applications. *Earth Space Sci.*, **6**, 1730–1748.

Schroedter-Homscheidt, M., A Drews, and S. Heise, 2008: Total water vapor column retrieval from MSG-SEVIRI split window measurements exploiting the daily cycle of land surface temperatures. *Remote Sens. Environ.*, **112**, 249–258.

Seemann, S. W., E. E. Borbas, R. O. Knuteson, G. R. Stephenson, and H.-L. Huang, 2008: Development of a global infrared land surface emissivity database for application to clear sky sounding retrievals from multi-spectral satellite radiance measurements. *Appl. Meteor. Climatol.*, **47**, 108–123.

Waldstreicher, J.S., 1989: A guide to utilizing moisture flux convergence as a predictor of convection. *Natl. Wea. Dig.*, **14**, 20–35.

Wimmers, A. J., and C. S. Velden, 2011: Seamless advective blending of total precipitable water retrievals from polar-orbiting satellites. *J. Appl. Meteor. Clim.*, **50**, 1024–1036.

REVIWER COMMENTS

[Authors' responses in *blue italics.*]

REVIEWER A (Rebekah B. Esmaili):

Initial Review:

Recommendation: Accept with minor revisions.

Summary: This study evaluates a new TPW algorithm that uses a three-LW channel method for calculating boundary-layer precipitable water (BPW) from GOES-R BT radiances. This study combines two methods: 1) a simultaneous temperature and moisture retrieval using an RTE; and 2) a channel differencing methods from 10.35 µm, 11.2 µm, and 12.3 µm, which have a small attenuation difference for water vapor when the lapse rate is non-zero. While this would provide a geophysical retrieval, the first method requires a sounding instrument to be successful. A caveat of this second method is that at these wavelengths, the surface contribution to the signal can be significant and lead to errors in the final WV product. Furthermore, the retrieved value is not geophysical, but a BT difference. The authors developed a scheme that incorporates these two methods to retrieve BPW while minimize the methods limitations. The authors developed a set of RTEs that solve for skim Temperature and TPW simultaneously. 11 and 12 um are the split window region, and 10 um makes it possible retrieve low level.

The authors evaluate the BPW product for clear-sky fields of view only. They perform a type of "cloud clearing" over 3×3 array of TPW pixels, with an AVHRR cloud mask product when available and when not, they employ a simple 10.35 µm brightness temperature threshold. The authors note that errors can exist near cloud edges. A challenge of this approach is that the depth of the column is unknown/the weighting functions change from scene to scene. Thus, it is confusing to assigning a measure of integrated precipitable water. To determine the "depth" of the PW, the authors compared to the totals of 50-m layers of PW and determined the BPW is in <1.5 km (≈850 hPa). At higher values, the errors increase after that. The authors then show a case study of how their product can be used to see fine, low level moisture structure that later developed into a convection. In addition to convection, the authors highlight that this product may provide value for mesoscale and regional scale meteorological phenomena and would be useful for model verification.

[Substantive] Comments: I think this work is interesting and innovative, I appreciate the simplicity of the approach and could see it being used as part of the suite of ABI channels and "differencing" products (e.g. sandwich) already used by forecasters. The number of applications does seem a bit narrow but by working with forecasters, they may identify future needs and test some of their potential applications (e.g., mesoscale convergence in Florida / evolution of boundary-layer moisture return east of the Rockies). These examples might be easier to follow with an illustration or even better, visual support.

This product was designed with convective forecasting in mind. We hope to continue interactions with forecasters to come up with other applications for the product, along with specific examples.

Figure 3: This figure really should include error bars. Further, the discussion surrounding this figure should be expanded to include typical summer boundary layer depth at both day and night. Is this a realistic "boundary layer" over the region studied? What regions/scenarios is the BPW less representative for surface water due to BL height (either too low or too high?)? Are there any other known caveats when used in practice during optimal conditions (e.g. clear sky)?

In regards to Fig. 3, the x-axis, root mean square error, is itself related to the magnitude of the error bars. The plot should not be understood as a measure of boundary layer height, but the minimum of the curve at 1450 m corresponds to the height for which the integrated precipitable water is most likely equal to the BPW product value (i.e., the height with the smallest error bars). That it is not known how high up from the surface the BPW product is measuring the water vapor is a weakness in the product. It is almost always (95%) representative of the lower levels in some sense, however. More discussion of Fig. 3 was

added, as well as a suggestion of a more in depth, radiosonde-by-radiosonde study for future work to further understand "typical" and "atypical" cases in regards to a comparison with the morphology of the temperature and moisture profile.

Perhaps the name of the product needs to be reconsidered for future work. The name "boundary-layer precipitable water" may be misleading as it is not the amount of water vapor in the boundary layer as defined meteorologically, but rather the amount of water vapor near the surface of the earth as defined radiatively. That is, it is the amount of water vapor detected by longwave infrared window channels, the weighting functions of which peak near the surface. The term boundary-layer precipitable water is appropriate in that the water vapor measured will be largely near the surface, like the meteorologically defined boundary layer, but it is not the amount of water vapor in the boundary layer per se.

As far as other caveats are concerned, two come to mind that are addressed in the paper. Finding out what is causing the low bias over land at night is the first priority. Emissivity variations should be investigated to see if including them is worth the extra effort to incorporate the additional dataset.

BPW in data assimilation: While I am not familiar with decisions surrounding the RAP, I would like to know how realistic this claim is. My understanding is that for most (all?) other NCEP models, is that products are never assimilated. If there is no discussion taking place between researchers on both teams, I think this is speculation and shouldn't be included in the paper. I do agree that the statement that this product can be useful for model verification and this is a valuable way to use this data. "The product's high spatial and temporal resolution track the locations of moisture needed for thunderstorm development. Alternatively, the detailed location of the dry air may provide utility in determining where thunderstorms are not likely to occur." Are there any examples of the second, "alternative" scenario?

Yes, we probably overplayed the role that the BPW product might currently play in operational data assimilation. There are research efforts in data assimilation, of course, which may be more likely to investigate the pros and cons of assimilating products. The text was altered to suggest the possibility rather than imply anything certain.

As far as examples of dry air hindering the development of thunderstorms, the text was changed to mention development or maintenance, then pointed again the thunderstorm to the southwest of the primary thunderstorm in western Kansas on 15 June 2017. After it developed it moved into drier air, which likely acted to weaken the storm.

[Minor comments omitted...]

Second Review:

Recommendation: Accept.

General Comment: I looked through the paper and edits, and I have nothing further to add. The authors addressed all my previous comments.

REVIEWER B (Timothy J. Schmit):

Initial Review:

Recommendation: Accept with minor revisions.

Overview: The authors are to be commended how they are moving from the use of GOES-16 ABI from single and multi-spectral imagery applications, to more quantitative applications and at fine spatial scales. This is a good approach to get more information / use from the ABI.

Substantive Comments: Page 2, Given its wide use, please include this reference on the MIMIC microwave TPW product:

Wimmers, A. J., and C. S. Velden, 2011: Seamless advective blending of total precipitable water retrievals from polar-orbiting satellites. *J. Appl. Meteor. Climatol*., **50**, 1024–1036.

Reference included.

More recently Dr. Li and others have shown that not only cloud-free regions can be retrieved but also in regions of thin clouds, hence consider to reference:

Li, Z., J. Li, W. P. Menzel, J. P. Nelson III, T. J. Schmit, E. Weisz, and S. A. Ackerman, 2009: Forecasting and nowcasting improvement in cloudy regions with high temporal GOES Sounder infrared radiance measurements. *J. Geophys. Res. Atmos.*, **114**, D09216, doi:10.1029/2008JD010596.

Reference included.

Please include this reference, which covers the pros and cons of generation TPW from the ABI:

Schmit, T., J. Li, J. Gurka, M. D. Mitch K. J. Schrab, J. Li, and W. F. Feltz, 2008: The GOES-R Advanced Baseline Imager and the continuation of current sounder products. *J. Appl. Meteor. Climatol*., **47**. 2696–2711.

Recall that the ABI was only considered to generate TPW, after the cancellation of the high-spectral IR sounder on the GOES-R series.

Reference included.

While it's true that the GOES-R series does not include a high-spectral-resolution infrared sounder, I think it's important to remind the readers that had been the plan for many years, until HES was canceled in 2007. This is why the atmospheric profiles from the ABI are called "legacy". Stated another way, when HES was cancelled, using the ABI to continue certain observations such as TPW was the only option to provide a continuation of products that where generated from the legacy GOES sounder. More on the legacy sounder:

Schmit, T. J., W. F. Feltz, W. P. Menzel, J. Jung, A. P. Noel, J. N. Heil, J. P. Nelson, and G. S. Wade, 2002: Validation and use of GOES sounder moisture information. *Wea. Forecasting*, **17**, 139–154.

Mention of HES cancellation and reference included.

While it is true that moisture will cause the 12 μm to be colder than the 11 μm, other factors can cause this as well, such as dust. Please include something on this. For example, inversions, dust, instrument noise, etc.

The lapse-rate issue was already mentioned in that section, and signal to noise was brought up in Section 2b. A statement on dust was added.

Given that the operational moisture profiles and TPW are available from NOAA NESDIS, please include some comparisons between that existing operational product and this new product. For example, in Fig. 3, compare to the operational values for the same cases. While it is true that the operational retrieval version uses a first guess, the comparisons would be good information to include. I recall the TPW specs for accuracy and precision were 1 and 3 mm, respectively, which are being met. Please reference:

Schmit, T. J., and Coauthors, 2019: Legacy atmospheric profiles and derived products from GOES-16: Validation and applications. *Earth Space Sci*., **6**, 1730–1748.

An additional figure comparing the BPW to GOES LAP TPW was included, as well as the Schmit et al. 2019 reference.

What were the times of the radiosondes that were compared to? Only 18 UTC? If so, this should be stated.

Change made to explicitly state that radiosondes are between 17 and 22 UTC.

What are the surface emissivity differences between the bands used? Seems that unity is assumed for both land and water? The value should be less for the pixels over the land. Also, could consider using a surface emissivity database, such as:

Seemann, S.W., E. E. Borbas, R. O. Knuteson, G. R. Stephenson, and H.-L. Huang, 2008: Development of a global infrared land surface emissivity database for application to clear sky sounding retrievals from multi-spectral satellite radiance measurements. *J. Appl. Meteor. Climatol.*, **47**, 108–123.

Yes, one of the suggested next steps is to investigate a variable surface emissivity over land. The Seemann et al. 2008 reference was included, and a specific reference to the assumption of unit emissivity used by Chesters, Uccellini, and Robinson was included. The idea was to start simple—all that is currently needed are the three GOES-ABI images.

In June of 2017, the GOES-16 ABI was not yet deemed operational. At the very least, this fact should be stated, that the system was at the provisional stage. Ideally, a case study from an operational time would be used.

Mention of the checkout period in Section 2b was made more explicit.

This statement "Previous attempts at measuring the low-level water vapor from a geostationary imager used only two channels, one near 11 μm and near 12 μm, as those were the only split-window channels available" should be amended to include the current ABI atmospheric profiles, which use around 8 infrared bands.

That statement was made in the context of low-level water vapor products that did not rely on a full retrieval. I adjusted the text to make that explicit.

Some mention should be given to the ideal of combining information from GEO and (high-spectral) LEO to profile forecasters with a single set of profiles, using information from both sensors.

It is not clear that the discussion of combined GEO/LEO retrieval techniques is necessary in this work. The generation of full temperature and moisture profiles from LEO and GEO platforms were mentioned to set the stage for what is of interest here: computing only low-level water vapor from GOES-16 in a way that is both reasonably accurate, and that takes full advantage of the spatial and temporal benefits afforded by the geostationary platforms. Using data from polar-orbiting and geostationary satellites to produce a combined retrieval requires quite a bit of spatial and temporal matching, complexities that may produce an accurate retrieval of the full atmosphere, but is not really what is of interest here.

[Minor comments omitted...]

Second Review:

Recommendation: Accept with minor revisions.

General comment: The authors addressed my main issues, small items remaining…

[Minor comments omitted...]